Phase-shifting birefringent scatterplate interferometer

Michael B. North-Morris, Jay VanDelden, and James C. Wyant

We realized what we believe is a new phase-shifting scatterplate interferometer by exploiting the polarization characteristics of a birefringent scatterplate. The common-path design of the interferometer reduces its sensitivity to environmental effects, and phase shifting allows quick and accurate quantitative measurements of the test surface. A major feature of the birefringent scatterplate approach for phase shifting is that no high-quality optical components are required in the test setup. The theory of the interferometer is presented, the procedure for the fabrication of the birefringent scatterplate is described, and experimental results are shown. © 2002 Optical Society of America

OCIS codes: 120.3180, 120.3940, 120.5050, 120.6650.

1. Introduction

The most significant advancement in interferometry and other types of instrumentation over the past 30 years has been the development of the computer. The prime manifestation of this occurrence in optical testing has been the evolution of phase-shifting interferometry. Phase-shifting interferometry records a series of interferograms while the reference phase is changed. The wave front is encoded in the irradiance distribution of the fringe pattern, and a simple point-by-point calculation in the computer recovers the phase. Some of the advantages of phase-shifting interferometry over other measurement techniques are high measurement accuracy, rapid measurement capability, and good results with low-contrast fringes. Accuracies of the order of 1/1000 of a wave are achievable. Phase-shifting interferometry was first conceived by Carré[1] in 1966 and was more fully developed later by Crane,[2] Bruning et al.,[3] and Wyant[4] to name a few. Unfortunately, there is a limit imposed on every measurement technique. For phase-shifting interferometry the limiting error is usually fringe movement caused by vibrations and index variations in the optical path.

Common-path interferometers are one possible solution to the environmental limitations. Their common-path design makes them largely insensitive to vibrations and index variation in the optical path. Unfortunately, because the test and reference beams traverse the same optical path, it is difficult to separate the test and reference beams for phase shifting.

A few clever groups have phase shifted common-path interferometers with varying success. Kwon, who fabricated a point-diffraction interferometer onto a sinusoidal grating, was the first to phase shift the point-diffraction interferometer.[5] The diffraction orders contained the desired phase shift. Later Mercer et al.[6] produced a phase-shifted point-diffraction interferometer by embedding a microsphere into a thin liquid-crystal layer. The microsphere created the reference beam, and the liquid crystals produced a variable phase shift. Most recently the point-diffraction interferometer was phase shifted by Medecki et al.[7] In this setup the beam coming from the test optic is divided into two beams with a small angular separation by use of a grating. The zero-order beam focuses onto a small pinhole creating the reference, and the first-order beam passes directly through a much larger hole that is slightly offset from the pinhole. The phase shift is created when the grating is shifted laterally.

The scatterplate interferometer has also been successfully phase shifted by two research groups: Huang et al.[8] and Su and Shyu.[9] Both methods exploit polarization to separate the test and reference beams when an auxiliary optic is placed near the test
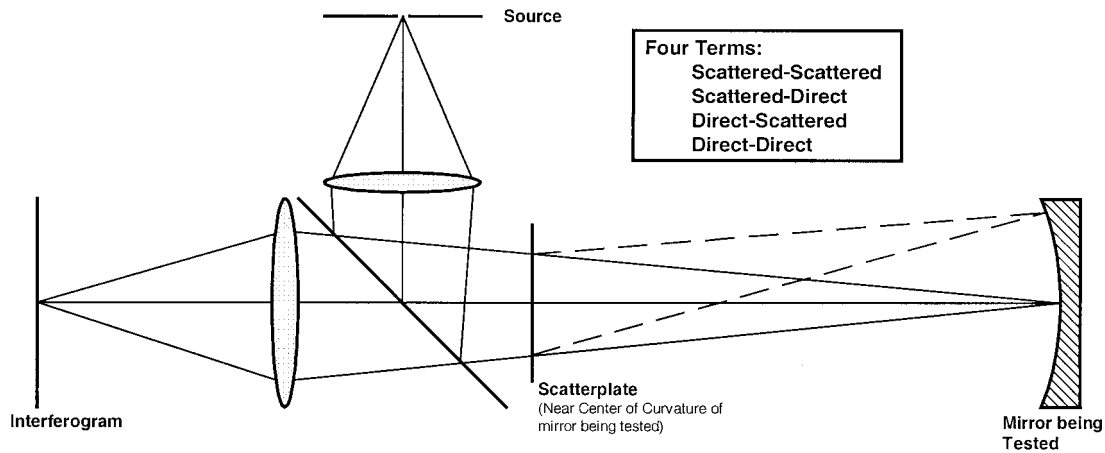
Fig. 1. Scatterplate interferometer for the testing of concave mirrors.

mirror. Huang *et al.* placed a small quarter-wave plate near the test surface that rotated only the incident linear polarization of the reference beam by 90°. With orthogonal polarizations in the test and reference beams, the interferometer is phase shifted with an electro-optic light modulator. Su and Shyu, playing on the same theme, placed a large polarizer with a small hole in the center near the test surface. In combination with additional polarization manipulating optics, the polarizer rotates the polarization of the test beam 90°.

The phase-shifting scatterplate interferometer presented in this paper also uses polarization to separate the test and reference beams. However, it does not require optics to be placed near the test surface. The secret to this more practical approach is use of a birefringent scatterplate to separate the test and reference beams.

2. Conventional Scatterplate Interferometer

A. Common-Path Interferometer

Because of its common-path design and unique ability to average many measurements at one time, the scatterplate interferometer is the ideal choice for a phase-shifting common-path interferometer. The scatterplate interferometer belongs to a subset of interferometers known as common path. As the name implies, a common-path interferometer is one in which the test and reference beams traverse nearly the same optical path. The advantages of common-path interferometers are well documented[10–14]: (1) reduced sensitivity to vibrations and air turbulence, (2) no precision auxiliary optics required, and (3) a white-light source can be used.

Because both the test and the reference beams travel the same path, it is easy to imagine that, for the most part, both beams experience the same phase variations that are due to optical path perturbations brought on by vibrations and air turbulence. Less obvious is the absence of piston error; relative longitudinal motion between the interferometer and the test optic introduces defocus only, which is usually

undetectable if the vibration movements are small.[13] Another advantage of the common-path design is the ability to use moderate-quality optics in the interferometer. The aberrations present in the illumination and imaging optics will primarily affect the test and reference beams equivalently. In addition, common path also implies equal path, accordingly white-light sources can be used. There are, however, limitations imposed on the source size and spectral distribution.[13]

In addition to being common path, the scatterplate interferometer has the unique property of averaging many measurements at one time. Because each scatter point on the scatterplate scatters the light in a unique manner, each scatter point makes a statistically independent measurement of the surface under test, and the resulting interferogram is an average of all the measurements. Any small spatial phase variations present in the beam incident on the scatterplate will be averaged, significantly reducing the errors associated with them.

B. Qualitative Description of Scatterplate Interferometer

The scatterplate interferometer is schematically a simple design. The configuration for the testing of spherical mirrors is shown in Fig. 1. A small circular aperture is illuminated with a laser or broadband source producing a source of limited extent for the interferometer. A focusing lens is used to image the source onto the test mirror by way of a beam splitter that removes the source from the path of the return beam and a scatterplate. The scatterplate is placed at the center of curvature of the test mirror. Part of the light incident on the scatterplate scatters, illuminating the entire mirror surface; part of it passes directly through, imaging to a point on the test mirror. After reflecting off the test surface the light again propagates through the scatterplate, scattering a portion of the beam. Finally a focusing lens is used to image the interference fringes onto a screen or detector.

The question now arises, if all the light travels the same path, what is interfering to produce fringes?

To answer the question it is necessary to look more closely at the effect of the scatterplate. Each time the light encounters the scatterplate, some of it is scattered and a portion passes directly through the plate. Because the scatterplate is traversed twice, there are four permutations of the beam that arrive in the image plane: (1) scattered–scattered, (2) scattered–direct, (3) direct–scattered, and (4) direct–direct. An examination of each of these combinations will uncover their role in producing fringes. The direct–direct beam passes directly through the scatterplate both times it is encountered, forming an image of the source called the hot spot in the image plane. Because the hot spot is never scattered, it does not contribute to the production of interference fringes. Similarly, the scattered–scattered beam does not play a role in the formation of interference fringes. The light is scattered both times it passes through the scatterplate, producing background irradiance in the image plane. If a laser source is used, the background irradiance, as well as the interference fringes, will contain a speckle pattern. The direct–scattered beam is the reference beam of the interferometer. The light passes directly through the scatterplate on the first pass and forms an image of the source on the test surface. If the image of the source is small enough, the phase variations introduced into the beam on reflection are negligible. On the return leg the light is scattered. The scattered–direct beam serves as the test beam of the interferometer. The light is scattered on its initial pass through the scatterplate, illuminating the entire test mirror. Any departures from a sphere will introduce phase variations in the beam. The light then passes directly through the scatterplate, producing fringes when it interferes with the reference beam.

It seems unlikely that two beams of light that have been scattered at different positions in the interferometer could possibly produce interference fringes. In general, the process described above would not produce interference fringes; however, Burch[10] came up with the solution: The scatterplate must have inversion symmetry. Inversion symmetry means that each scatter point has an exact twin located directly opposite the center point of the scatterplate. Figure 2 shows an example of inversion symmetry designed into a binary photomask used to expose scatterplates. The reason inversion symmetry works is revealed when we examine individual scatter points and their effect on the reference and test beams. Keep in mind that an examination of individual points is not the complete story. Summing the wave fronts from all the scatter points forms the contour fringes. Figure 3(a) summarizes the effect of inversion symmetry for a perfectly aligned system. When the incident light interacts with the scatterplate, the light scattered at scatter point $S(x, y)$ acts like a point source. Because the scatterplate is located at the center of curvature of the test mirror, point $S(x, y)$ is imaged back into the plane of the scatterplate at the conjugate point $S'(x, y)$. The reference beam passes directly through the scatterplate,
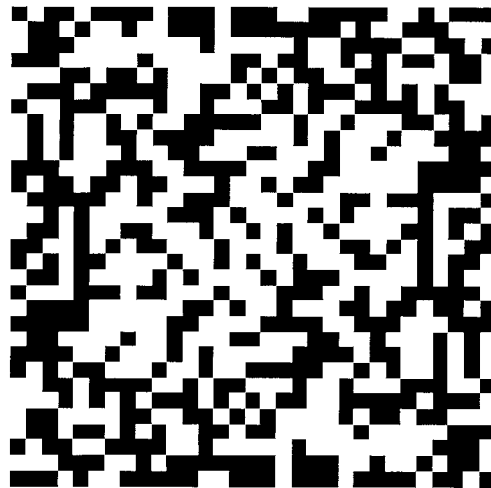

Fig. 2. Inversion symmetry designed into a binary scatterplate.

reflects off the test mirror, and scatters at point $S(-x, -y)$. With inversion symmetry and proper alignment, point $S(x, y)$ and $S(-x, -y)$ are scattered in exactly the same manner, and the test and reference beams both appear as point sources located at point $S(-x, -y)$. As a result, the phase change that is due to scattering is the same for both beams.

The above discussion of inversion symmetry is for a system with perfect alignment, but this is not always the case. The effect of misalignment of the scatterplate is now discussed. Lateral movement of the scatterplate produces tilt in the contour fringes. Figure 3(b) demonstrates the consequence of when the center point of the scatterplate is placed above the center of curvature of the test mirror. The image of $S(x, y)$, although still in the plane of the scatterplate, no longer coincides with the symmetric point $S(-x, -y)$. The result is tilt in the contour fringes produced by the interference of two laterally shifted point sources. Similarly, longitudinal misalignment of the scatterplate adds defocus to the contour fringe pattern. Figure 3(c) shows the effect of when the scatterplate is placed inside the center of curvature of the test mirror. The image of point $S(x, y)$ is still at the same lateral position as the symmetric point $S(-x, -y)$; however, it no longer lies in the plane of the scatterplate. The interference of the two longitudinally shifted point sources produces defocus in the contour fringes. Adjusting the scatterplate position adds an important flexibility that enables us to minimize the number of contour fringes across the image plane. Figure 4 contains typical fringe patterns obtained with the scatterplate interferometer. The fringe patterns contain varying amounts of tilt and defocus. Note that the fringe patterns contain speckle as is consistent with use of a coherent source.

3. Phase-Shifting Scatterplate Interferometer

A. Birefringent Scatterplate

Before the operation of the interferometer as a whole can be understood, it is necessary to independently
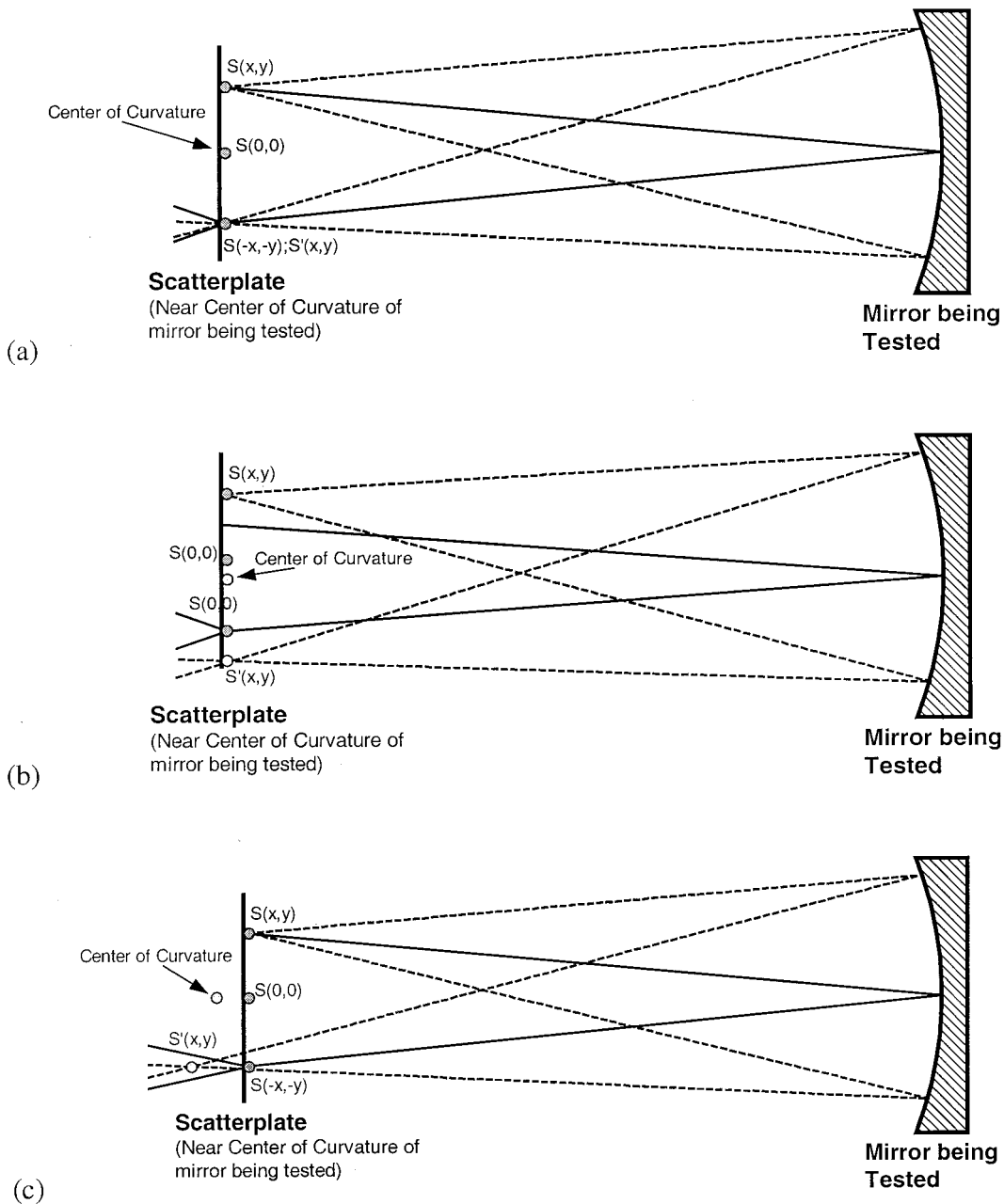
Fig. 3. Point-to-point analysis of inversion symmetry: (a) perfect alignment, (b) lateral misalignment of scatterplate, (c) longitudinal misalignment of scatterplate.

examine the characteristics of the birefringent scatterplate. In the phase-shifting scatterplate interferometer, the goal is to control when the test and reference beams are scattered. Here the birefringent scatterplate shown in Fig. 5 provides the desired control. The appropriate aperiodic pattern with inversion symmetry is etched into a calcite retarder with a chemical etching process. An index-matching oil chosen to match the ordinary index of the crystal is then pressed between the calcite and a glass slide. The end result is that, for light polarized along the ordinary axis of the crystal, the index of the oil and the index of the crystal appear the same and

the light passes directly through the scatterplate, whereas light polarized along the extraordinary axis of the crystal sees an index difference and is scattered by the rough surface. This is the property that supplies the control over scattering that is necessary to phase shift the scatterplate interferometer.

Matching the index of the oil with the ordinary index of the calcite is fairly straightforward. However, it is important to consider the dispersion of both materials. Literature usually quotes the indices of refraction at the sodium D line. Unfortunately, matching the indices at 589 nm does not guarantee that the indices will match at a different wavelength.
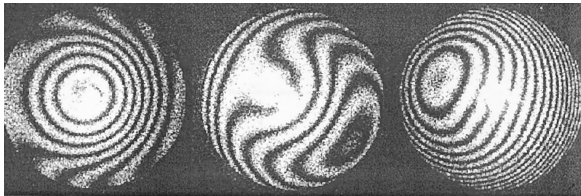
Fig. 4.   Typical scatterplate interferograms.

The dispersion of calcite is described by the following equations[15]:

$$n_o(\lambda)^2 = 1 + \frac{0.8559\lambda^2}{\lambda^2 - (0.0588)^2} + \frac{0.8391\lambda^2}{\lambda^2 - (0.141)^2}$$
$$+ \frac{0.0009\lambda^2}{\lambda^2 - (0.197)^2} + \frac{0.6845\lambda^2}{\lambda^2 - (7.005)^2}, \quad (1)$$

$$n_e(\lambda)^2 = 1 + \frac{1.0856\lambda^2}{\lambda^2 - (0.07897)^2} + \frac{0.0988\lambda^2}{\lambda^2 - (0.142)^2}$$
$$+ \frac{0.317\lambda^2}{\lambda^2 - (11.468)^2}, \quad (2)$$

where λ is the wavelength of the source in micrometers. The manufacturer usually supplies the wavelength dependence of the index-matching oil. The dispersion equation for Cargille's $n_d = 1.662$ oil is

$$n_{1.662} = 1.621298 + \frac{1192615}{(\lambda 10^4)^2} + \frac{7.658881 \times 10^{12}}{(\lambda 10^4)^4}. \quad (3)$$

At the operating wavelength of 633 nm, the indices differ by only 0.00005.

When the index of the oil is matched with the ordinary index of the calcite rather than the extraordinary index, the ordinary index does not change for oblique illumination of the birefringent scatterplate. This is an important advantage because the scatterplate will be placed in a converging beam, and index matching is crucial to the operation of the phase-shifting birefringent scatterplate interferometer.

B.   Qualitative Description of Phase-Shifting Scatterplate Interferometer

It is instructive to examine the operation of the phase-shifting scatterplate interferometer qualitatively. The schematic diagram of the interferometer is shown in Fig. 6. If the polarization elements such as the wave plates and polarizers are removed, it is a conventional scatterplate interferometer. The polarizer passes linearly polarized light oriented at 45° with respect to the optic axis of the calcite scatterplate, providing equal amplitudes for the component of the beam polarized along the optic axis and the component polarized orthogonal to the optic axis. The component parallel to the optic axis will see the extraordinary index of the crystal, and the perpendicular component will see the ordinary index. A liquid-crystal retarder produces a variable phase
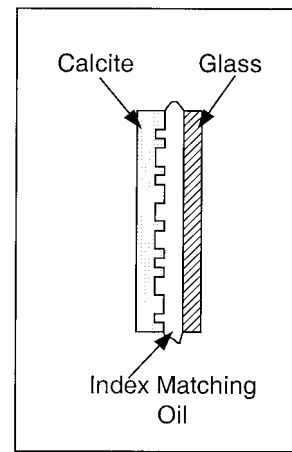

Fig. 5.   Birefringent scatterplate.

shift between the two orthogonal components of polarization, and the rotating ground glass plate reduces the speckle in the interferogram because it effectively enlarges the apparent source size. The rotating ground glass plate is offset slightly from the intermediate image of the source such that the diameter of the incident beam is larger than the original source. At each point of the rotating ground glass plate the phase of the scattered light is changing rapidly compared to the integration time of the CCD array. The result is an extended source, made up of incoherent point sources, that is, the same size as the beam incident on the ground glass plate. We can adjust the size of the source and consequently the coherence by longitudinally shifting the rotating ground glass plate. The source created at the ground glass plate is imaged onto the test mirror. The scatterplate is located at the center of curvature of the test mirror and scatters only the component of the beam that is polarized parallel to the optic axis of the crystal. The perpendicular component passes through the scatterplate and forms an image of the source on the test mirror. Both the scattered and the direct beams pass through a quarter-wave plate twice producing a 90° rotation in the direction of polarization of each. As a result, on the second pass through the scatterplate the beams change roles: The one that traveled directly through on the first pass is now scattered, and the one that was scattered now passes directly through. The outcome is a scattered–direct and direct–scattered beam with orthogonal polarization. Note that, if there is no unwanted scattering when the beams pass directly through the scatterplate, there is no background irradiance in the interference pattern. Similarly, if all the light is scattered by the scatterplate on the passes when scattering is wanted, the hot spot will not exist. In general, not all the light polarized parallel to the optic axis is scattered, and the quarter-wave plate does not rotate the two polarizations exactly 90°. Consequently, both orthogonal polarization components will contain a direct–direct and
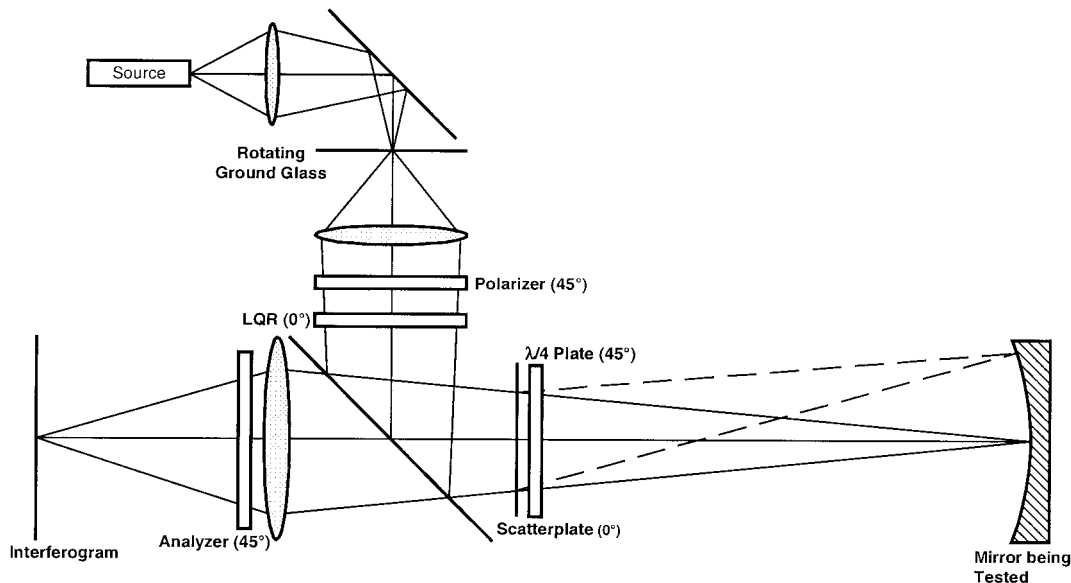
Fig. 6. Phase-shifting scatterplate interferometer. LQR, liquid-crystal retarder.

scattered–scattered element producing a hot spot and background irradiance in the interference pattern. Finally, the test mirror is imaged onto a CCD array through an analyzer, which serves to combine the test and reference beams for observation of interference fringes. The end result is that we can phase shift the interference fringes by applying a voltage to the liquid-crystal retarder. Figure 7 contains a series of four shifted interferograms.
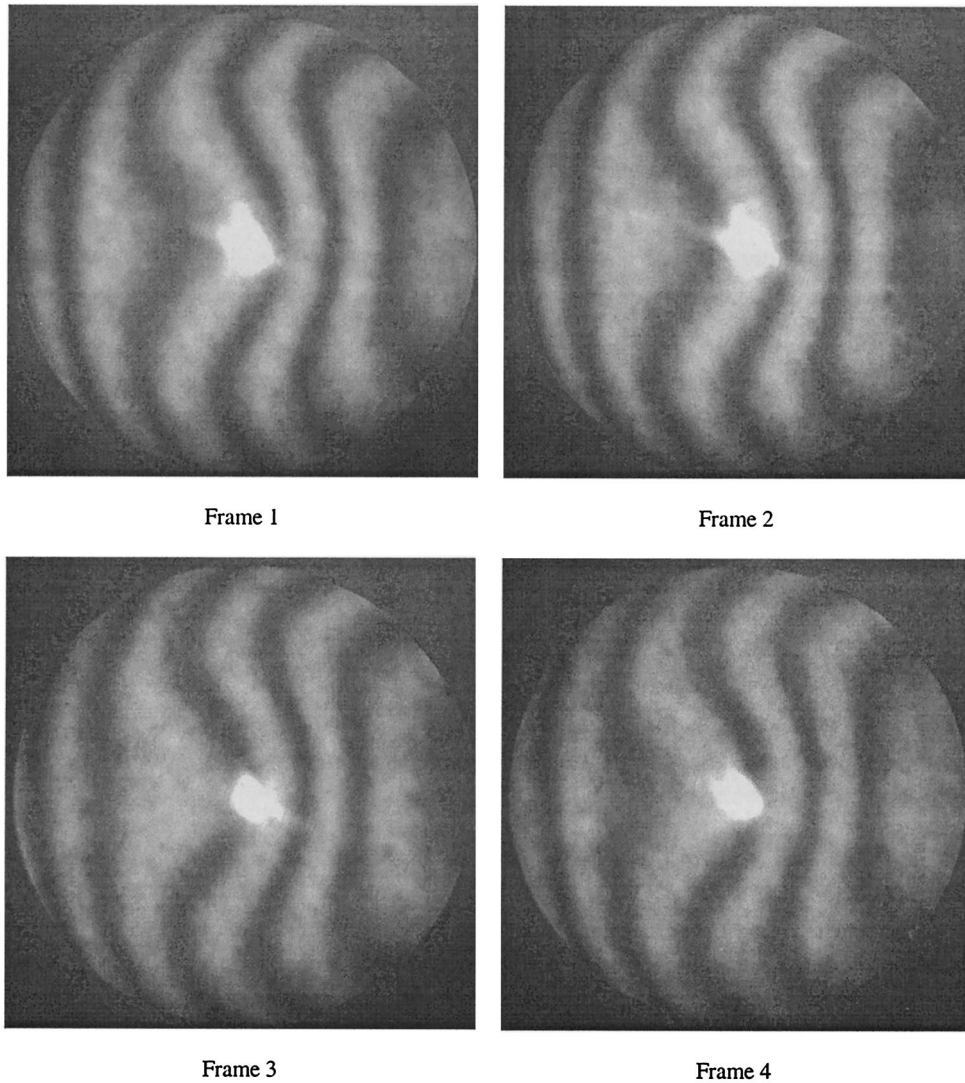
4. Scatterplate Manufacture

The birefringent scatterplate is the key component of the phase-shifting scatterplate interferometer presented in this paper. In this section we discuss its manufacture. There are many issues to be considered, including pattern generation, average feature size, inversion symmetry, and etching rates. We address each of these issues in the context of describing the entire manufacturing process. First, an overview of the entire process is presented in general terms. Then we provide a detailed presentation for exposing the scatterplate pattern using two different methods.

A. Manufacturing Process

Because the operation of the interferometer depends on the birefringent properties of the scatterplate, it is necessary to etch the scatterplate pattern directly into the birefringent material. The process presented here will work for most birefringent materials; however, the chemicals used to clean and etch the scatterplate may vary. Etching precise patterns into birefringent materials is a new concept, and to our knowledge there is no literature to speak of that outlines a process. The recipes presented here are specific to calcite and were obtained through trial and error.

The birefringent scatterplate is made by a six-step etching process outlined in Fig. 8. First, a good quality wave plate made with calcite is cleaned in four stages with acetone, isopropanol, deionized water, and a plasma chamber. The calcite is placed in each of the chemicals in the order listed above for 30 s and agitated gently. Upon removal from the deionized water, the calcite is dried and placed in a plasma chamber for 30 s to remove any remaining impurities on the surface. If the substrate is not clean, the photoresist will not adhere to the surface. The next step in the manufacturing process is to spin coat the sample with photoresist. There are many photoresists available with different viscosities and sensitivities. Shipley's 1813 photoresist was used because of its availability. We coated the scatterplate with photoresist by spinning it at 500 rpm for 5 s and increasing the speed to 5000 rpm for 30 s. The speed and duration of the spin coating, as well as the viscosity, determine the thickness of the deposited photoresist. For this application the thickness of the photoresist is not critical provided that it stands up to the chemical etching. After coating, the sample is soft baked on a hot plate for 1.5 min at 100 °C to solidify the photoresist. The scatterplate pattern is then exposed into the photoresist by use of either a speckle pattern or a photomask. Developing removes the photoresist from the calcite only in the regions that are exposed with flux levels above 150 mJ/cm^2. We developed the pattern by placing it in Shipley's 352 developer for 45 s and rinsing in deionized water for 1 min. After developing, the sample is hard baked for another 1.5 min on the hot plate. The birefringent scatterplate is then chemically etched with an extremely weak solution of hydrochloric acid. A 37% solution of HCl is diluted 5000 to 1 in deionized water, and the scatterplate is gently agitated in the solution for 3–5 min depending on the etch depth desired. Figure 9 shows a plot of the etch

Frame 1

Frame 2

Frame 3

Frame 4

Fig. 7.   Phase-shifted fringe patterns.

depth as a function of etching time for calcite.   Rinsing the calcite in deionized water for 1 min terminates the chemical etching.   Finally, the photoresist is removed by the same cleaning process used to clean the blank substrate.   Figure 10 shows a surface plot of an etched scatterplate.

B.   Holographic Exposure

A common method to expose scatterplates is to double expose a speckle pattern, in which the scatterplate is rotated 180° between each exposures.[13]   Figure 11 shows the holographic setup used to expose scatterplates.   An argon-ion laser beam tuned to a wavelength of 458 nm is expanded with a beam expander. The beam is then scattered by a ground glass plate, and a speckle pattern is created in the film plane. The size of the smallest features in the speckle pattern is determined by the diameter of the beam incident on the ground glass plate and the distance from the ground glass to the film plane.   In turn, the size of the speckle pattern features determines the
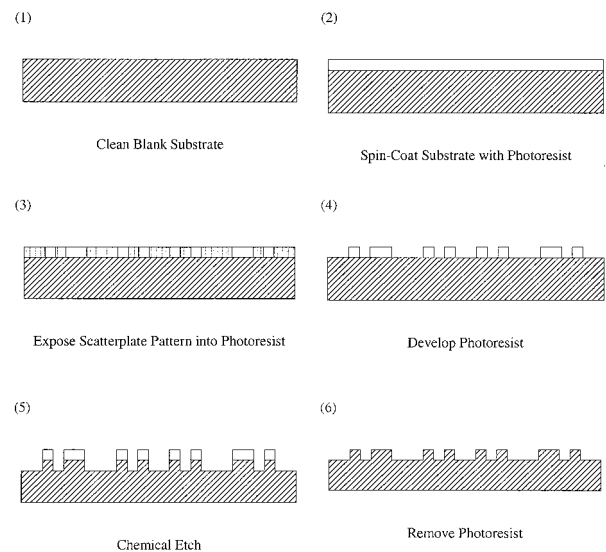

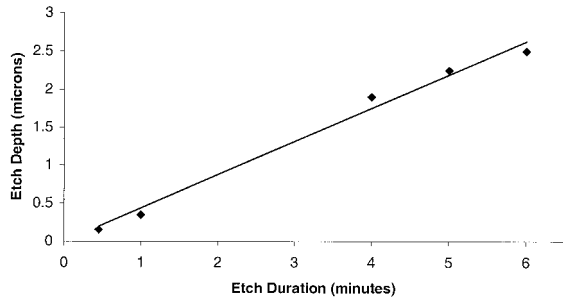Fig. 8.   Scatterplate manufacturing process.

Fig. 9. Etch depth versus etch time for calcite in diluted HCl.

f/number of the mirror that can be measured. The photoresist-coated sample is placed in the film plane and rotated 180° between two exposures. The rotation is controlled by a kinematic mount, shown in Fig. 11, to ±0.05°. The end result is a random pattern with inversion symmetry.

A simple geometric analysis will reveal the relationship between the holographic setup and the f/number of the mirror that can be measured. There are two geometries to consider in this analysis. First, the exposing geometry will determine the smallest feature size on the scatterplate, and then the geometry of the scatterplate interferometer will determine the fastest mirror that can be tested. Figure 12 shows both geometries. When the speckle
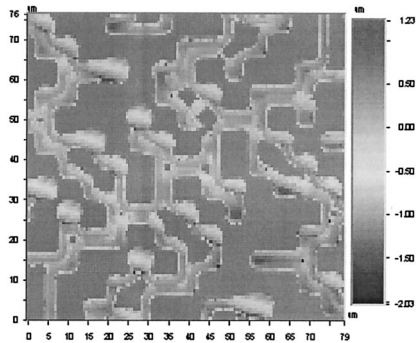

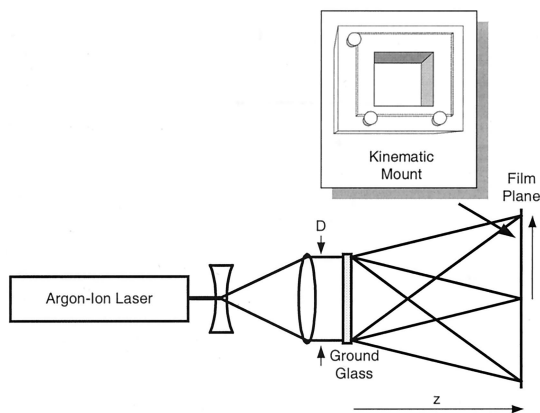Fig. 10. Surface plot of birefringent scatterplate manufactured with a photomask.

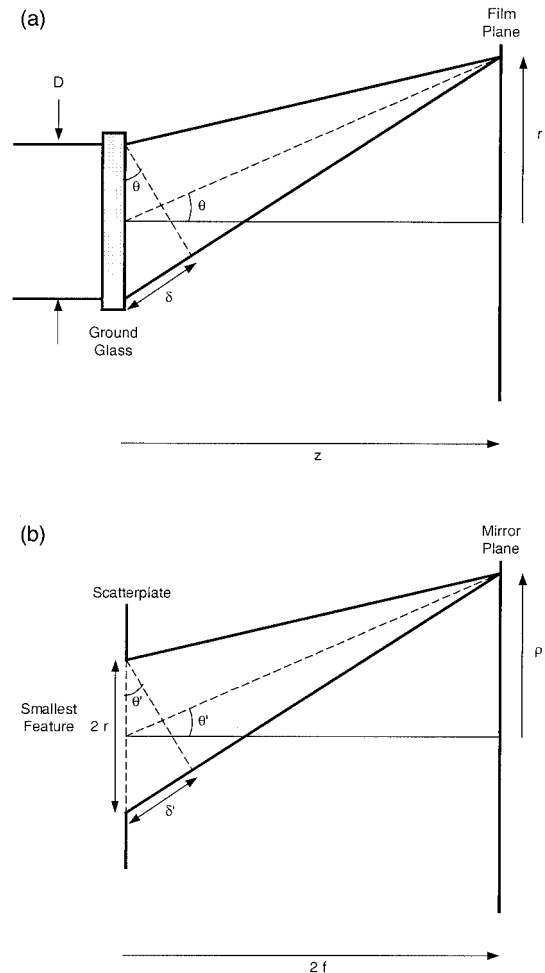Fig. 11. Holographic exposure of a scatterplate.

Fig. 12. f/number analysis for holographic exposure: (a) recording geometry, (b) interferometer geometry.

pattern is exposed, interference between the two most widely separated points on the ground glass produces the smallest features. We can determine the radius of the smallest features by finding the first interference minimum off the optical axis. For the geometry shown, the radius is given by

$$r = \frac{z\lambda}{D}, \qquad (4)$$

where z is the distance from the ground glass plate to the film plane, λ is the wavelength of the source, and D is the diameter of the beam incident on the ground glass plate. The analysis for the scattered light is similar except that the smallest features on the scatterplate are used to determine the radius at which the irradiance at the mirror falls off to zero. Repeating the analysis for the interferometer geometry and substituting for r, we obtain the desired relation:

$$f/\text{number} = \frac{z}{2D}, \qquad (5)$$

where

$$f/\text{number} = \frac{f}{2\rho}. \tag{6}$$

Here ρ is the radius of the mirror aperture and f is the focal length of the mirror. The ratio of z over D determines the f/number of the mirrors that can be measured by use of the exposed scatterplate. In a practical measurement, it is not desirable to have the irradiance drop off significantly at the edge of the mirror. If the minimum f/number is half of the f/number of the test mirror, the irradiance will drop by 50% at the edge of the test mirror.

The advantage of using the holographic exposure is that we can easily create low f/number scatterplates. The disadvantage is the elaborate setup required for each exposure and the possible errors in symmetry that are due to the rotating of the scatterplate between exposures.

C. Photomask

A better method to expose the scatterplates is to use a photomask. A photomask is a glass substrate on which the desired pattern is written into chrome with an electron beam. Once the pattern is written, the photomask can be used repeatedly to manufacture many scatterplates. The photomask is placed in close contact with the photoresist-coated sample, and illumination of the sample with a UV source exposes the pattern. The exposing is usually done with an apparatus known as a mask aligner and takes only a few minutes. With one photomask many scatterplates can be rapidly exposed. Most of the work associated with use of a photomask is in its design.

As with the holographic exposure, the feature sizes in the mask determine the f/number of the mirror that can be measured with that particular scatterplate. It turns out that, for a randomly generated pattern, the average feature size in one dimension is two pixels and the minimum feature size is one pixel. Because the irradiance pattern at the mirror is the squared modulus of the Fraunhofer diffraction pattern of the scatterplate and the shape of the smallest feature is known, the f/number can be determined when we take the Fourier transform of the smallest feature in the mask. The fastest mirror that can be completely illuminated is one for which the envelope of the irradiance pattern drops to zero at the edge of the mirror. The envelope function is given by

$$E_{\text{envelope}} = \left| \text{FF} \left[\text{rect}\left(\frac{x}{a}\right) \text{rect}\left(\frac{y}{a}\right) \right] \right|^2$$
$$= |a^2 \, \text{sinc}(a\xi)\text{sinc}(a\eta)|^2$$
$$= a^4 \, \text{sinc}^2(a\xi)\text{sinc}^2(a\eta), \tag{7}$$

where

$$\xi = \frac{x}{\lambda f}, \tag{8}$$

$$\eta = \frac{y}{\lambda f}. \tag{9}$$

Here f is the focal length of the test mirror, a is the width of the smallest feature, and λ is the wavelength of the source. The irradiance pattern drops to zero at

$$x = \frac{\lambda f}{a}, \tag{10}$$

which gives the following relation for the minimum f/number:

$$(f/\text{number})_{\text{min}} = \frac{a}{2\lambda}. \tag{11}$$

In a practical measurement, it is not desirable to have the irradiance drop off significantly at the edge of the test mirror. As a rule of thumb, a scatterplate should be designed such that the minimum f/number is one half of the f/number of the test mirror.

The photomask patterns are generated when a two-dimensional array is randomly filled with ones until approximately 25% of the array is full. Then a copy of the array is created, rotated 180°, and summed with the original. Pixels with values greater than one are set equal to one. The final pattern is an array of ones and zeros that are pseudorandom with inversion symmetry. The size of the pixels can be specified when the pattern is sent to the photomask manufacturer.

An $f/6$ mirror with a focal length of 90.93 cm was measured for the results presented in Section 6. We fabricated the scatterplate used for the measurement using a photomask with 4-μm pixels. At 633 nm the minimum f/number was 3.16, approximately half of the f/number of the mirror. The overall dimensions of the scatterplate were 8 mm $\times$ 8 mm.

5. Experimental Results

The best way to estimate the accuracy of an interferometer is to measure a known surface or, equivalently, compare measurements with a calibrated instrument. Figure 13(a) contains a surface plot of the test mirror obtained by the phase-shifting scatterplate interferometer, and Fig. 13(b) shows a surface measurement of the same mirror acquired with a commercial phase-shifting Fizeau interferometer. Because of the long focal length of the test mirror and the limited size of the isolation table, a folding flat was used in the Fizeau measurement. In double pass, the possible peak-to-valley error in the measurement created by the flat was 0.073 waves. Despite the measurement uncertainty because of the folding flat, the scatterplate and Fizeau measurements compare well. The peak-to-valley difference is less than 0.035 waves.

A second method to determine the performance is to establish the repeatability of the interferometer by the subtraction of two consecutive measurements. The rms difference between two consecutive mea-

(a)

Surface Statistics:
Ra: 46.78 nm
Rq: 55.31 nm
Rz: 237.37 nm
Rt: 251.29 nm

Set-up Parameters:
Size: 451 X 431
Sampling: 0.00 mm

Processed Options:
Terms Removed:
None
Filtering:
None

(b)

Surface Statistics:
Ra: 47.53 nm
Rq: 55.31 nm
Rz: 215.52 nm
Rt: 231.40 nm

Set-up Parameters:
Size: 184 X 220
Sampling: 0.00 mm

Processed Options:
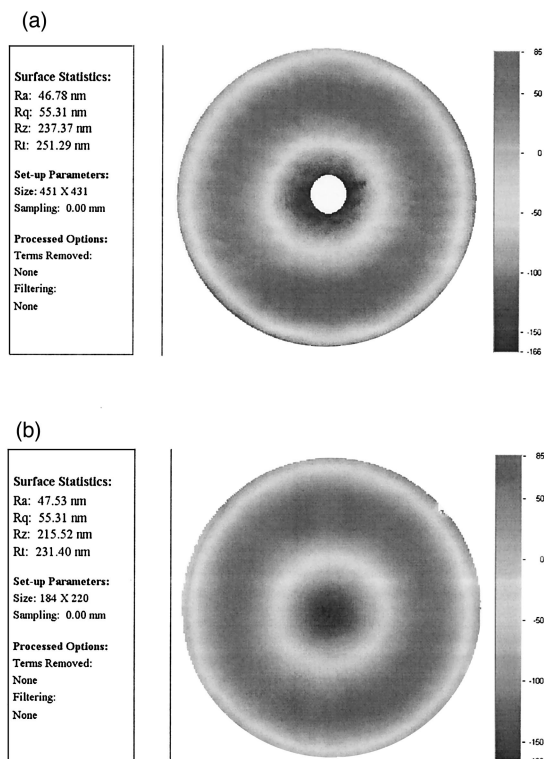Terms Removed:
None
Filtering:
None

Fig. 13. (a) Surface measurement taken with a phase-shifting scatterplate interferometer. (b) Surface measurement taken with a Wyko 6000 phase-shifting Fizeau interferometer.

surements was found to be of the order of 0.0025 waves.

6. Discussion

In this paper we described and analyzed a new phase-shifting scatterplate interferometer. The interferometer separates the test and reference beams by exploiting the polarization characteristics of a birefringent scatterplate. The birefringent scatterplate was manufactured with the pattern etched into a good quality calcite wave plate. The scatterplate scatters only the component of polarization oriented along the extraordinary axis of the crystal. Together with two polarizers and a quarter-wave plate, the birefringent scatterplate produces test and reference beams with orthogonal polarizations. A variable phase shift is induced between the beams by use of a liquid-crystal retarder.

The performance of the interferometer was admi-

rable. Subtracting two consecutive measurements demonstrated a repeatability of 0.0025 waves rms, and a comparison of the measurements with a commercial interferometer established a peak-to-valley accuracy of 0.035 waves, which was well within the uncertainty of the commercial interferometer measurement.

References

1. P. Carré, "Installation et Utilisation du Comparateur Photo-electrique et Interferentiel du Bureau International des Poids de Mesures," Metrologia **2**, 13–16 (1966).
2. R. Crane, "Interference phase measurement," Appl. Opt. **8**, 538–542 (1969).
3. J. H. Bruning, D. R. Herriott, J. E. Gallagher, D. P. Rosenfeld, A. D. White, and D. J. Brangaccio, "Digital wavefront measuring interferometer for testing optical surfaces and lenses," Appl. Opt. **13**, 2693–2703 (1974).
4. J. C. Wyant, "Use of an ac heterodyne lateral shear interferometer with real-time wavefront correction systems," Appl. Opt. **14**, 2622–2626 (1975).
5. O. K. Kwon, "Multichannel phase-shifted interferometer," Opt. Lett. **9**, 59–61 (1984).
6. C. R. Mercer, K. Creath, and N. Rashidnia, "A phase-stepped point diffraction interferometer using liquid crystals," in *Interferometry VII: Techniques and Analysis*, M. Kujawinska, R. J. Pryputniewicz, and M. Takeda, eds., Proc. SPIE **2544**, 87–93 (1995).
7. H. Medecki, E. Tejnil, K. A. Goldberg, and J. Bokor, "Phase-shifting point diffraction interferometer," Opt. Lett. **21**, 1526–1528 (1996).
8. J. Huang, T. Honda, N. Ohyama, and J. Tsuiiuchi, "Fringe scanning scatter plate interferometer using a polarized light," Opt. Commun. **68**, 235–238 (1988).
9. D.-C. Su and L.-H. Shyu, "Phase-shifting scatter plate interferometer using a polarization technique," J. Mod. Opt. **38**, 951–959 (1991).
10. J. M. Burch, "Scatter fringes of equal thickness," Nature (London) **171**, 889 (1953).
11. J. M. Burch, "Interferometry in scattered light," in *Optical Instruments and Techniques*, J. H. Dickson, ed. (Oriel, London, 1970), pp. 220–229.
12. R. M. Scott, "Scatterplate interferometry," Appl. Opt. **8**, 531–537 (1969).
13. L. Rubin, "Scatterplate interferometry," Opt. Eng. **19**, 815–824 (1980).
14. J. T. Rässänen, K. Peiponen, K. M. Abedin, K. Tenjimbayashi, T. Eiju, and K. Matsuda, "Integrated scatter plate and projection lens for scatter plate interferometer," Rev. Sci. Instrum. **69**, 1587–1590 (1998).
15. W. J. Tropf, M. E. Thomas, and T. J. Harris, "Properties of crystals and glasses," in *Handbook of Optics*, M. Bass, ed. (McGraw-Hill, New York, 1995), Vol. 2, pp. 33.1–33.101.